



# Model investigation of NO<sub>3</sub> secondary organic aerosol (SOA) source and heterogeneous organic aerosol (OA) sink in the western United States

J. L. Fry and K. Sackinger

Department of Chemistry, Reed College, Portland, OR, USA

Correspondence to: J. L. Fry (fry@reed.edu)

Received: 15 December 2011 – Published in Atmos. Chem. Phys. Discuss.: 17 February 2012

Revised: 6 September 2012 – Accepted: 12 September 2012 – Published: 28 September 2012

**Abstract.** The relative importance of NO<sub>3</sub>-initiated source and heterogeneous sink of organic aerosol in the western United States is investigated using the WRF/Chem regional weather and chemistry model. The model is run for the four individual months, representing the four seasons, of January, May, August, and October, to produce hourly spatial maps of surface concentrations of NO<sub>3</sub>, organic aerosol (OA), and reactive organic gases (ROG, a sum of alkene species tracked in the lumped chemical mechanism employed). These “baseline” simulations are used in conjunction with literature data on secondary organic aerosol (SOA) mass yields, average organic aerosol composition, and reactive uptake coefficients for NO<sub>3</sub> on organic surfaces to predict SOA source and OA heterogeneous loss rates due to reactions initiated by NO<sub>3</sub>. We find both source and sink rates maximized downwind of urban centers, therefore with a varying location that depends on wind direction. Both source and sink terms are maximum in summer, and SOA source dominates over OA loss by approximately three orders of magnitude, with large day-to-day variability. The NO<sub>3</sub> source of SOA (peak production rates of 0.4–3.0 μg kg<sup>-1</sup> h<sup>-1</sup>) is found to be significantly larger than the heterogeneous sink of OA via NO<sub>3</sub> surface reactions (peak loss rates of 0.5–8 × 10<sup>-4</sup> μg kg<sup>-1</sup> h<sup>-1</sup>).

Dockery, 2006), and a significant but poorly understood climate forcing agent (IPCC, 2007). Aerosols affect Earth’s radiative balance by scattering and absorbing sunlight, and by influencing cloud formation and lifetime. The uncertainty in the overall climate forcing by aerosols arises because knowledge is incomplete on the mechanisms of their production and loss. These source uncertainties are particularly large for that fraction of aerosol that is nitrate (Karydis et al., 2007; Yu et al., 2005) or organic aerosol (OA) (Hallquist et al., 2009), the latter of which comprises a substantial fraction of sub-micron aerosol globally (Kanakidou et al., 2005). A major fraction of OA is secondary, that is, formed by gas-to-particle conversion in the atmosphere, with source estimates varying from 50–910 TgC yr<sup>-1</sup> (Hallquist et al., 2009). Higher numbers arise from top-down estimates than from bottom-up estimates, suggesting either that chamber experiments underestimate secondary organic aerosol (SOA) production from volatile organic compound (VOC) oxidation processes, or that heterogeneous aerosol loss processes are disproportionately affecting chamber experiments, relative to the real atmosphere.

One candidate for additional SOA production is the reaction of nitrate radical (NO<sub>3</sub>) with biogenic VOCs, which comprise the majority of non-methane hydrocarbons emitted to the atmosphere (Guenther et al., 2006). Although present in low concentrations (10 s of pptv) and primarily at night, NO<sub>3</sub> is highly reactive with alkenes and therefore disproportionately responsible for the oxidation of biogenic VOCs, which all contain at least one double bond. Isoprene and the major monoterpenes ( $\alpha$ -pinene,  $\beta$ -pinene,  $\Delta$ -carene, and

## 1 Introduction

Atmospheric aerosols (liquid or solid particles suspended in air) are both an important air pollutant, with adverse visibility (Watson, 2002) and human health effects (Pope and

limonene) have a significantly shorter lifetime with respect to  $\text{NO}_3$  than either OH or  $\text{O}_3$ , when normalized to average 24-hour concentrations of each oxidant (Atkinson and Arey, 2003). SOA formation from these reactions have received sparser study, but the available experimental evidence shows substantial aerosol yields: Griffin et al. (1999) measured mass yields for  $\text{NO}_3 + \Delta$ -carene (13–72%),  $\beta$ -pinene (32–89%) and sabinene (14–76%), with the large variation resulting from different initial BVOC concentrations. Hallquist et al. (1999) measured mass yield at lower BVOC concentrations of  $\approx 10$  ppb each for  $\alpha$ -pinene (<1%),  $\beta$ -pinene (10%),  $\Delta$ -carene (15%), and limonene (17%). More recently, Spittler et al. (2006) measured SOA mass yield from  $\text{NO}_3 + \alpha$ -pinene under atmospherically relevant, seeded conditions, to be on average 10%. Fry et al. (2009) measured the mass yield from  $\text{NO}_3 + \beta$ -pinene under atmospherically relevant conditions to be  $\approx 50\%$ .  $\text{NO}_3$ -initiated SOA yield from isoprene was recently investigated and found to be substantial: 4–24% for 20–100 ppb of isoprene (Ng et al., 2008) or 14% mass yield from 10 ppb isoprene, doubly nitrated (Rollins et al., 2009).

However,  $\text{NO}_3$  radical might also act as a *sink* for OA, through heterogeneous reactions on the surface of organic particles that can result in revolatilization of some organic mass. Molina et al. (2004) demonstrated the possibility of such revolatilization in the case of OH radical, showing rapid consumption of alkane and aromatic organic monolayers, with an effective lifetime with respect to volatilization of  $\approx 6$  days. Laboratory studies have shown substantial uptake coefficients of  $\text{NO}_3$  radical on organic surfaces (Moise et al., 2002; Gross et al., 2009; Gross and Bertram, 2008), and at least one recent study has focused on laboratory measurements of volatilization of an organic layer by  $\text{NO}_3$  (Knopf et al., 2006), finding that in the case of alkanes, only 10% of a monolayer was volatilized under the most polluted conditions. We expect this volatilization process would be more rapid with alkenes, given the 2 orders of magnitude higher uptake coefficients.

If efficient volatilization occurs, this heterogeneous reaction of  $\text{NO}_3$  on the surface of OA may be important for atmospheric aerosol lifetimes. However, even if this is not a significant removal process for OA, it may yet be important as a loss mechanism for gas-phase NOy. In this paper, we model the  $\text{NO}_3$ -initiated source of SOA and the sink process of  $\text{NO}_3 + \text{OA}$ , examining the latter both from the standpoint of atmospheric organic aerosol budgets and NOy budgets.

## 2 Model description

For this study, the WRF-Chem model was run for four months, January, May, August, and October, using the same chemical mechanism, to capture seasonal variation in background chemistry. Surface spatial maps of nitrate radical concentration and several volatile and aerosol-phase lumped or-

ganic species are used to construct spatial maps of  $\text{NO}_3$ -initiated SOA source and  $\text{NO}_3$ -initiated consumption of OA, to assess processes governing nighttime NOy sink, and whether  $\text{NO}_3$  is a greater net source or sink of organic aerosol in the western U.S.

### 2.1 WRF-Chem model runs

The fully coupled online regional chemical/dynamical Weather Research and Forecasting/Chemistry (WRF-Chem) model is employed to generate hourly spatial maps of relevant chemical species as inputs to offline calculations of SOA source and sink via nitrate radical ( $\text{NO}_3$ ). WRF is a mesoscale numerical weather prediction model developed as a collaboration between federal agencies, headed by the National Center for Atmospheric Research (NCAR), designed for operational forecasting and atmospheric research (<http://www.mmm.ucar.edu/wrf/users/>). Meteorological initial and boundary conditions were obtained from re-analysis data available from the National Centers for Environmental Prediction (<http://www.emc.ncep.noaa.gov/mmb/rrean/>). In addition to the dynamical calculations of winds, temperatures, water partitioning, etc. included in the model physics, a chemical mechanism is fully coupled at each time step (Grell et al., 2005). This adds calculation of surface emissions, including online calculation of biogenic emissions, gas phase chemistry, radiation and photolysis rates (Wild et al., 2000).

The version of the model employed here uses anthropogenic emissions at 4 km resolution from the EPA's 2005 National Emissions Inventory (<http://www.epa.gov/ttnchie1/net/2005inventory.html>) and calculates biogenic emissions online based on the scheme developed by Guenther and others (Grell et al., 2005; Guenther et al., 1993, 1994; Simpson et al., 1995; Schoenemeyer et al., 1997). This emissions scheme calculates emissions of isoprene, monoterpenes, and other volatile organic compounds based on USGS land use category, temperature, and radiation. These emissions are subsequently split into the chemical species available in the chosen chemical mechanism and added as a source term to the chemical processor. This disaggregation calculation also relies on land use types, splitting e.g. the monoterpene emissions differentially among internal (OLI) and terminal (OLT) olefins in the chemical mechanism depending on the land type. The Guenther module apportions the majority of monoterpene emissions to the internal olefin variable (OLI) (80–98%, depending on which of the 24 USGS land use types, e.g. grassland, coniferous or deciduous forest).

The chemical mechanism employed was the CBMZ mechanism (Zaveri and Peters, 1999), comprising 164 reactions among 67 chemical species. The aforementioned internal and terminal olefin lumped hydrocarbon species (OLI and OLT) and the individually treated isoprene (ISOP) comprise all the reactive (i.e., non-aromatic) alkenes in the gas-phase mechanism, and hence are the hydrocarbon species of interest for  $\text{NO}_3$  gas-phase reaction. To this was added aerosol treated

using the MOSAIC model (Zaveri et al., 2008) with aerosols grouped into 4 sectional bins (0.0390625–0.15625 μm, 0.15625–0.625 μm, 0.625–2.5 μm, and 2.5–10 μm), adding an additional 64 variables to describe the chemical composition (9 composition types, including organic carbon (OC)) and number/optical properties of these 4 size bins. For this study, this model was run for a domain covering the western United States (lat: 30.3 to 49.5° N, lon: –112.30 to –126.7° W), with a horizontal resolution of 12 km by 12 km, and 26 vertical levels, non-uniformly spaced, from the surface to 110 mbar. Only the surface data is employed for further analysis.

This model was run for the months of January, May, August of 2008 and October 2004, for a domain covering the western United States. From these month-long model runs, we extract hourly surface spatial maps of [NO<sub>3</sub>] (ppb) and organic aerosol particulate concentration (WRF-Chem variables oc\_a01, oc\_a02, oc\_a03, and oc\_a04, in μg kg<sup>-1</sup>), nighttime hours only, for the offline calculations described below.

## 2.2 NO<sub>3</sub> OA source and sink calculations

Two MATLAB programs were written to estimate aerosol formation and loss rates due to NO<sub>3</sub> oxidation. Both programs retrieve data from WRF output files and perform calculations in loops that repeat for each 1-h timestep and terminate according to user-specified time brackets. The results are then averaged over time and plotted by color on a map.

### 2.2.1 Modeling NO<sub>3</sub> SOA source

Chamber studies have determined aerosol mass yields for a variety of oxidant-VOC pairs. Table 1 shows the species and corresponding mass yields used to estimate SOA formation from NO<sub>3</sub>, as well as rate constants for these reactions. We note that because these yield data are taken from experiments conducted at ≈10 ppb of starting VOC, they may be higher than many ambient locations. We further note that the SOA source in this model is treated as nonvolatile; we do not allow NO<sub>3</sub>-produced SOA to repartition. Sensitivity studies are conducted (see Sect. 3.3) to assess the effect a lower yield would have on our conclusions. The source program begins each loop by retrieving data from the WRF file on the concentrations of NO<sub>3</sub> and the selected VOCs (OLI, OLT, ISOP) in each geographic pixel and converting into appropriate units for the given rate constants. This calculation assumes that essentially all OLI are α-pinene and all OLT are β-pinene, a simplification that we expect represents the bulk of the VOCs in the west coast domain reasonably well, as these are the dominant monoterpenes emitted from coniferous forests. However, the NEI-based anthropogenic emissions module employed in these WRF-Chem runs does emit some small reactive anthropogenic alkenes (e.g. propene) into these olefin species. For example, in the extreme case of downtown Los Angeles, inspection of emissions into WRF-

Chem shows that there is predicted to be approximately 10 times as much anthropogenic vs. biogenic OLT (OLI is more dominated by biogenics everywhere). Importantly, inspection of emissions variables in the model also reveals these anthropogenic OLI and OLT emissions to be highly localized to city centers. Because the observed peaks in NO<sub>3</sub> + VOC SOA production always occur downwind of urban centers and not directly over them, this source must be driven by the downwind maximum in NO<sub>3</sub> concentration. Therefore, this SOA formation occurs where local biogenic emissions dominate the reactive organic gases, so that the ROG (= OLI + OLT in the model) source driving aerosol formation in is unlikely to be substantially influenced by anthropogenic emissions.

The reaction rates are calculated using temperature data from the WRF output for each pixel where T-dependence is available, then multiplied by the percent mass yields of the respective reactions to give an aerosol formation rate in number of reactant molecules per second. These yields are then adjusted for the masses of the original reactants to obtain mass formation rates:

$$\text{rate} = k[\text{NO}_3][\text{VOC}] \quad (1)$$

$$\text{aero. mass form. rate} = \text{rate} \times \text{MW}_{\text{VOC}} \times \% \text{ mass yield} \quad (2)$$

At each WRF-Chem model timestep, we predict the magnitude of this rate and the corresponding NO<sub>3</sub> OA sink (described below). As an offline calculation aimed only at comparing the instantaneous rates of these processes, the OA produced by this source term is not added in to the model for the sink calculation.

### 2.2.2 Modeling NO<sub>3</sub> OA sink

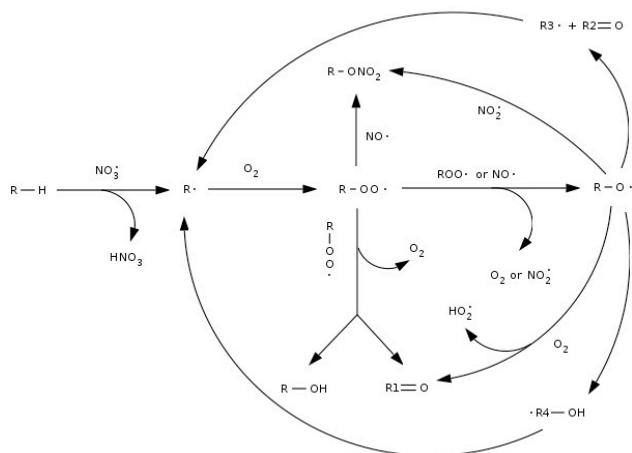
Uptake of OH is the rate-limiting step in heterogeneous OH oxidation (Molina et al., 2004). Since NO<sub>3</sub> has both lower uptake coefficients and lower atmospheric concentrations than OH (Gross et al., 2009), it is assumed that the rate-limiting step for NO<sub>3</sub> oxidation of an aerosol surface will likewise be NO<sub>3</sub> uptake. The reaction rate is therefore calculated using the following formula:

$$\text{rate}_{\text{uptake}} = \frac{\gamma \bar{c}(\text{NO}_3)}{4} \times \frac{\text{SA}_{\text{OA}}}{V_{\text{air}}} \times [\text{NO}_3] \quad (3)$$

where  $\gamma$  is the uptake coefficient on the surface of interest,  $\bar{c}$  is the average molecular speed of NO<sub>3</sub> (calculated from temperature in each pixel and molecular weight), and  $\frac{\text{SA}_{\text{OA}}}{V_{\text{air}}}$  is the surface area of organic aerosol per volume of air (defined below). An uptake coefficient of 0.1 was used for unsaturated (alkene) reaction sites and 10<sup>-3</sup> for saturated (alkane) sites, and the aerosol is considered to consist of 90% saturated carbons. These estimates are based on examination of the literature concerning organic aerosol composition (Alves et al., 2001; Baduel et al., 2010; Hamilton et al., 2004, 2006; Zhang et al., 2007) and NO<sub>3</sub> uptake coefficients on a variety

**Table 1.** Literature SOA mass yields from  $\text{NO}_3$  oxidation used in this model.

WRF/Chem species	Proxy	Mass yield	Rate constant ( $k$ ), $\text{cm}^3 \text{ molec}^{-1} \text{ s}^{-1}$
Isoprene (ISOP)	isoprene	14 %, Rollins et al. (2009)	$(3.03 \times 10^{-12}) e^{-446K/T}$ , Calvert et al. (2000)
Internal olefin (OLI)	$\alpha$ -pinene	10 %, Spittler et al. (2006)	$(1.19 \times 10^{-12}) e^{490K/T}$ , Calvert et al. (2000)
Terminal olefin (OLT)	$\beta$ -pinene	50 %, Fry et al. (2009)	$(2.41 \times 10^{-12})$ at 290 K, Calvert et al. (2000)

**Fig. 1.** Mechanism for  $\text{NO}_3$  oxidation of an alkane.

of surfaces (Moise et al., 2002; Knopf et al., 2006; Gross and Bertram, 2008; Gross et al., 2009). Aromatic species were not included due to a lack of sources for uptake coefficients and an estimated low prevalence in aerosol.

The sink program begins each loop by retrieving data from the WRF file on  $\text{NO}_3$  concentration, concentrations of total organic aerosol from all sources in four size bins, temperature, and air density. Using the simplifying assumption that organic aerosol exists in discrete droplets separate from other aerosol components, the surface area of organic aerosol ( $\text{SA}_{\text{OA}}$ ) per volume of air ( $V_{\text{air}}$ ) is calculated based on mass concentration of organic aerosol ( $\frac{m_{\text{OA}}}{m_{\text{air}}}$ ), densities of air ( $\frac{m_{\text{air}}}{V_{\text{air}}}$ ) and organic aerosol ( $\frac{m_{\text{OA}}}{V_{\text{OA}}}$ ), and average surface-area-to-volume ratios of the aerosol size bins,  $i$  ( $(\frac{\text{SA}_{\text{OA}}}{V_{\text{OA}}})_i$ ):

$$\frac{\text{SA}_{\text{OA}}}{V_{\text{air}}} = \sum_i \left( \frac{m_{\text{OA}}}{m_{\text{air}}} \right)_i \times \left( \frac{\text{SA}_{\text{OA}}}{V_{\text{OA}}} \right)_i \times \frac{V_{\text{OA}}}{m_{\text{OA}}} \times \frac{m_{\text{air}}}{V_{\text{air}}} \quad (4)$$

The density of organic aerosol is approximated at  $2 \text{ g cm}^{-3}$  (a rounded estimate for highly oxidized OA density, Hallquist et al. (2009)); all other quantities are retrieved from the WRF file or determined by the simulation parameters.

Because the organic aerosol taken at hourly intervals from the WRF-Chem simulation contains no information about functionalization, we use the reported organic mass to constrain the total surface area, but then apply estimates from the literature to generate an assumed carbon number distribution and functional group composition of this organic aerosol and

its reaction products, which can be interpreted as individual molecules for calculation of vapor pressures.

The products of the reaction are determined by the oxidation mechanisms shown in Figs. 1 and 2, assuming H abstraction from saturated sites and  $\text{NO}_3$  addition at unsaturated sites. Additional peroxide-forming reaction channels are known for alkylperoxy radicals (Calvert et al., 2000), but were not included because the products have comparatively low vapor pressures and thus do not conduce to an upper-limit estimate of volatilization. The branching ratio for the alcohol + carbonyl channel in both mechanisms is set at 0.6 (Knopf et al., 2006), while all other branches are assumed equally probable. Where applicable, it is assumed equally likely that a functional group will become part of a radical product or a stable product.

Calculations are performed as if every aerosol-phase organic molecule initially contains 2 hydroxyl groups and 1 carboxylic acid group. This level of functionalization agrees with mass spectrum data taken from the Pacific Northwest (Russell et al., 2010) for a 5-carbon molecule, while giving a reasonable OM/OC ratio of 1.7 for a 10-carbon molecule. The resulting types of products are shown in Figure 3 for a 7 carbon molecule. Fragmented products are constructed as averages, with half the carbon number of the parent molecule, one hydroxyl group, and a 50 % chance of acquiring the carboxylic acid. In order to avoid postulating products with more functional groups than carbons, 1–4 carbon molecules were excluded from a carbon number curve with mean 10 and standard deviation 5, and points on the curve were multiplied by 1.17 to result in an integral of unity from 5 to 20 carbons. While somewhat arbitrary, this simplification was considered acceptable since such low molecular weight compounds are less likely to be in the aerosol phase.

While the generation of this specified product matrix is required for calculation of gas/aerosol partitioning of the species and thus to determine an OA revolatilization rate, we wish to be clear that the assumptions invoked about initial composition and mechanism result in significant uncertainty in these products. The molecular structures represent our best guess, and the sensitivity calculations shown below in Sect. 3.3 are intended to help the reader evaluate the robustness of our conclusions with respect to these simplifying assumptions.

Using a vapor pressure calculator based on the SIMPOL group contribution method (Pankow and Asher, 2008), vapor pressures of the products shown in Fig. 3 were determined

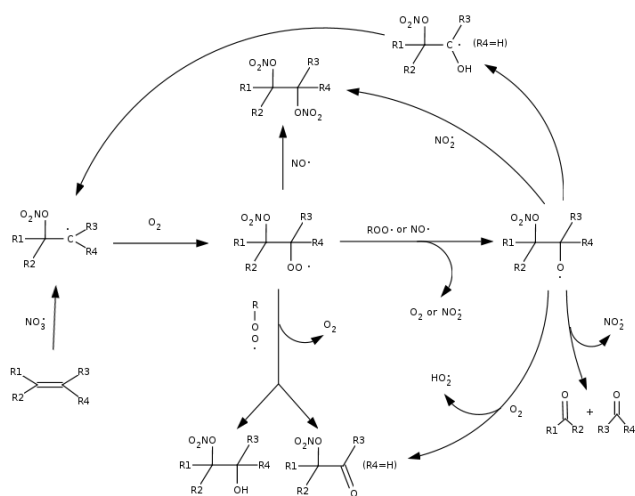


Fig. 2. Mechanism for NO<sub>3</sub> oxidation of an alkene.

at 290 K for carbon chain lengths from 5–20 (3–10 for fragmented products). Lone carbonyl groups were modeled as ketones rather than aldehydes. A table of the predicted vapor pressure of each possible molecular product, based on carbon chain length and combinations of functional groups is shown in the Supplement (Table S4).

The fraction of each product in the gas phase was calculated from partitioning theory. According to Odum et al. (1996), gas/aerosol partitioning of organic compounds obeys the following equation:

$$\frac{[\text{VOC}]_{\text{aero}}}{[\text{VOC}]_{\text{gas}}[\text{TSP}]} = \frac{760 R T f_{\text{OM}}}{\text{MW}_{\text{OM}} 10^6 \zeta P_{\text{vap}}} \quad (5)$$

where [TSP] is the total suspended particulate concentration in  $\mu\text{g m}^{-3}$ ,  $R$  is the ideal gas constant,  $8.206 \times 10^{-5} \text{ m}^3 \text{ atm mol}^{-1} \text{ K}^{-1}$ ,  $f_{\text{OM}}$  is the mass fraction of absorbing organic matter in the total suspended particulates,  $\zeta$  is the activity coefficient of the compound in the organic phase,  $\text{MW}_{\text{OM}}$  is the mean molecular weight of the absorbing organic phase, and  $P_{\text{vap}}$  is in Torr. We define  $f_{\text{OM}}[\text{TSP}] = [\text{OA}]$ , assume  $\zeta = 1$ , and rearrange to give an equation for the ratio ( $r$ ) of aerosol- to gas-phase VOC concentration:

$$r \equiv \frac{[\text{VOC}]_{\text{aero}}}{[\text{VOC}]_{\text{gas}}} = \frac{760 R T [\text{OA}]}{\text{MW}_{\text{OM}} 10^6 P_{\text{vap}}} \quad (6)$$

We also know:

$$[\text{VOC}]_{\text{aero}} + [\text{VOC}]_{\text{gas}} = [\text{VOC}]_{\text{total}} \quad (7)$$

Solving these equations for the volatile fraction, we find:

$$\frac{[\text{VOC}]_{\text{gas}}}{[\text{VOC}]_{\text{aero}}} = \frac{1}{r + 1} \quad (8)$$

With our functionalization parameters and carbon number curve,  $\text{MW}_{\text{om}}$  is about  $220 \text{ g mol}^{-1}$ , giving a constant factor

in Eq. (6) roughly equal to  $8.2 \times 10^{-8} \text{ Torr m}^3 \mu\text{g}^{-1}$ , giving:

$$r = 5 \times 10^{-8} \rho_{\text{air}} \frac{[\text{OA}]}{P_{\text{vap}}} \quad (9)$$

where  $P_{\text{vap}}$  is in Torr, [OA] is given in  $\mu\text{g kg}^{-1}$  dry air, and  $\rho_{\text{air}}$  is given in  $\text{kg m}^{-3}$ .

A limited number of products were classified as fully volatile or nonvolatile by observing that volatilization was greater than 99% or less than 1% under the range of [OA] conditions observed in the model ( $0.2 - 200 \mu\text{g kg}^{-1}$  dry air), corresponding to vapor pressure thresholds of  $1.6 \times 10^{-3}$  and  $1.6 \times 10^{-11}$  Torr.

The remaining semivolatile products are partitioned according to this scheme, based on the ratio of background organic aerosol to bin vapor pressure. The volatile fractions are then adjusted according to the mass of the original aerosol material (calculated from carbon number and functional groups) and carbon number prevalence.

### 3 Results and discussion

Spatial and seasonal variability in the NO<sub>3</sub> source and sink of aerosol can be observed in Figs. 4 and 5. The domain modeled includes the entire western United States, encompassing Washington, Oregon, California, Nevada, and parts of Idaho and Montana. In these figures, the center map in each row shows the overall source or sink rate ( $\mu\text{g kg}^{-1} \text{ h}^{-1}$ ) of organic aerosol due to the nitrate initiated mechanisms, flanked in each case by the spatial maps of the “reagents” from which the rate was calculated. For the source calculation, the reagents are NO<sub>3</sub> radical and reactive organic gases (ROG), which is a sum of the surface concentrations of the reactive alkenes: isoprene (ISOP) and the lumped alkenes internal (OLI) and terminal (OLT) olefins. For the sink calculation, the reagents are NO<sub>3</sub> radical and organic aerosol mass concentration. Each row corresponds to a one-month average of hourly nighttime-only concentrations: January, May, August, and October.

A summary of the observed temporal variation is shown in Table 2, which compares the peak source and sink rates in the western United States domain, calculated for the months of January, May, August, and October. The maximum in both source and sink rates is in the month of August, when surface concentrations of NO<sub>3</sub>, reactive organic gases, and organic aerosol are all at their maximum. Source rates always dominate over sink rates by three orders of magnitude.

In the western United States, the urban plumes of Seattle, Portland, San Francisco, and Los Angeles dominate the NO<sub>x</sub> emissions and therefore NO<sub>3</sub> sources, which appear in the downwind direction, where ozone production (and thus formation of NO<sub>3</sub> from NO<sub>2</sub> + O<sub>3</sub>) has maximized. For example, the Los Angeles NO<sub>3</sub> plume appears predominantly to the west over the Pacific Ocean in January, but predominantly to the east inland in spring, summer, and fall. Peak

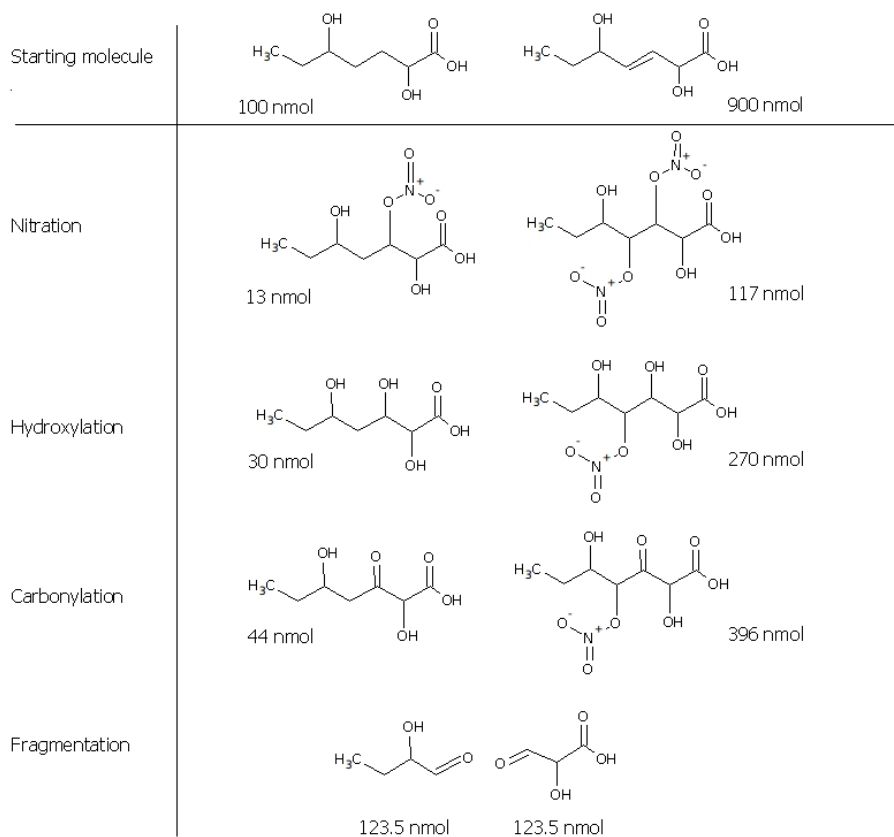


**Fig. 3.** Functional group composition of the products of 1  $\mu\text{mol}$  of 7-carbon model aerosol molecules, of which 10 % are saturated and 90 % unsaturated. We show quantitative yields of saturated (left) and unsaturated (right) molecules as predicted by the mechanism employed here.

**Table 2.** Summary of peak rates of  $\text{NO}_3$  initiated production and loss of aerosol over four seasons for the base case model.

Month	Maximum OA sink rate ( $\mu\text{g kg}^{-1} \text{h}^{-1}$ )	Maximum OA source rate ( $\mu\text{g kg}^{-1} \text{h}^{-1}$ )	Source Sink
Jan	$4.7 \times 10^{-5}$	0.4	8500
May	$2.6 \times 10^{-4}$	1.2	4300
Aug	$8.2 \times 10^{-4}$	3.0	3700
Oct	$1.7 \times 10^{-4}$	1.1	6500

organic aerosol production likewise occurs over urban areas in the WRF model, resulting in a spatial pattern similarly highlighting Los Angeles, Seattle, Portland, San Francisco, but also in this case Boise, Sacramento and Fresno. The reactive organic gases, in contrast, comprised dominantly of biogenic emissions, show a spatial pattern reflecting the locations of forests in the Pacific Northwest and northern California, and a strong seasonal maximum in spring/summer.

Details of the source and sink seasonal patterns are discussed below.

### 3.1 Seasonal variation in predicted $\text{NO}_3$ -initiated SOA source

Because the wintertime  $\text{NO}_3$  plume downwind of Los Angeles falls over the Pacific Ocean, the primary  $\text{NO}_3$ -initiated SOA source region in the January simulation is likewise over the ocean, as well as being of minimum magnitude (peak =  $0.4 \mu\text{g kg}^{-1} \text{h}^{-1}$ ) relative to the other seasons. A smaller source of  $0.10\text{--}0.15 \mu\text{g kg}^{-1} \text{h}^{-1}$  is more widely geographically dispersed, downwind (offshore) of the San Francisco bay area, in the Sierra Nevada mountains, Las Vegas, and east of Los Angeles.

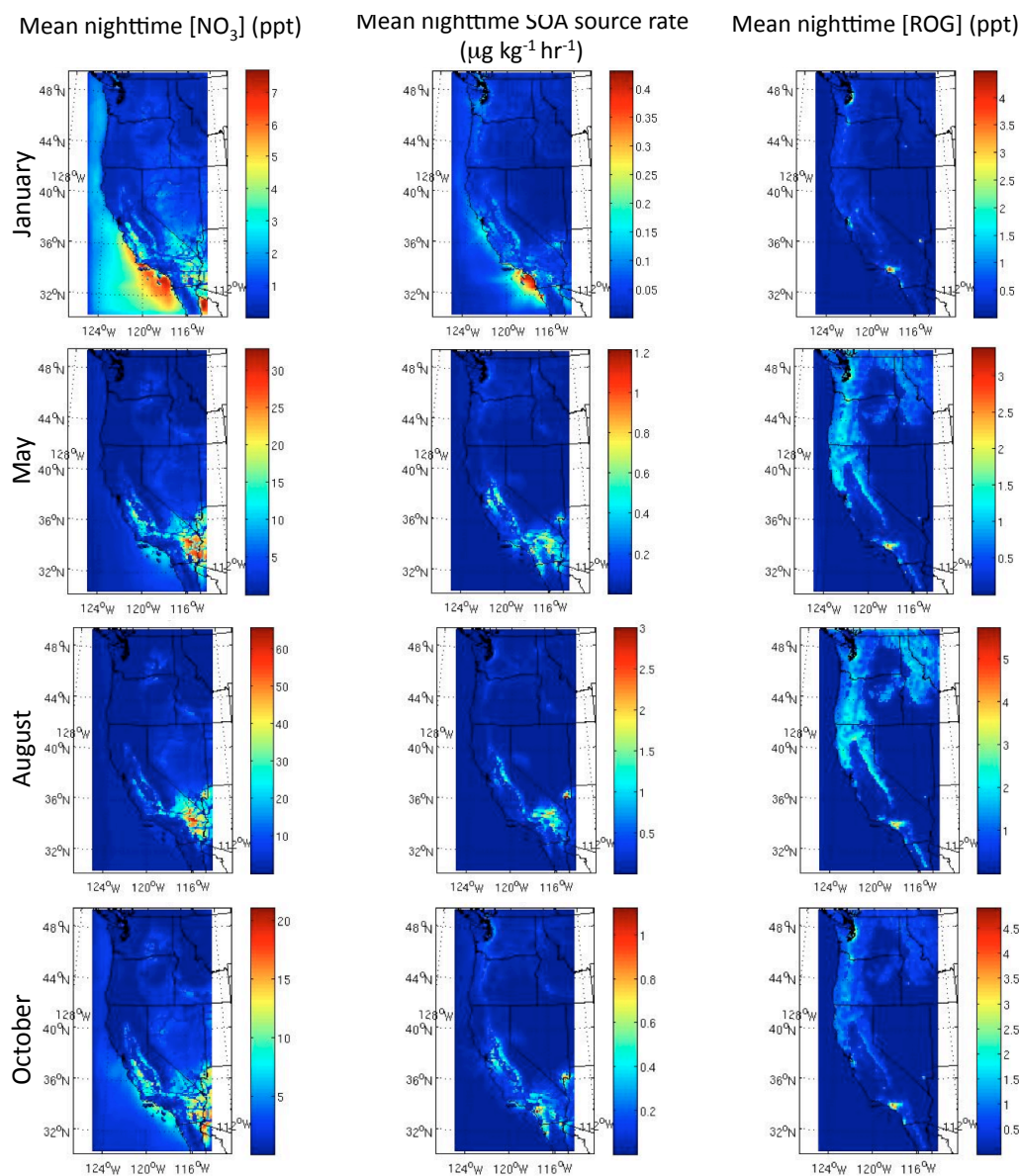


**Fig. 4.** Seasonal pattern of  $\text{NO}_3$ -initiated SOA source rate (center panels), which is calculated based on the hourly nighttime surface  $[\text{NO}_3]$  map (left panels) and surface reactive organic gases ( $[\text{ROG}]$ ) (right panels), which is a sum of isoprene (ISOP), internal (OLI) and external (OLT) olefins. The monthly average of these hourly calculations is shown here.

In spring (May simulation), the  $\text{NO}_3$ -initiated SOA source increases in the Sierra Nevada mountains east of San Francisco, east of Las Vegas, and a larger area east and southeast of Los Angeles, which is now downwind of these urban areas. The source rate in these regions is now in the range  $0.6\text{--}0.8\ \mu\text{g kg}^{-1}\ \text{h}^{-1}$ , with a peak of  $1.2\ \mu\text{g kg}^{-1}\ \text{h}^{-1}$  in east Los Angeles.

In summer (August simulation), the spatial pattern is similar but more biased eastward, as winds are more regularly onshore, and with larger source magnitude, especially east of Las Vegas. The Los Angeles downwind source is now

in the range of  $1\text{--}2\ \mu\text{g kg}^{-1}\ \text{h}^{-1}$ , and Las Vegas peaks at  $3\ \mu\text{g kg}^{-1}\ \text{h}^{-1}$ .

In fall (October simulation), the maximum source has shifted coastward again, with wind direction once again more mixed. Peak SOA production in inner east Los Angeles is  $1\ \mu\text{g kg}^{-1}\ \text{h}^{-1}$ , with the broader regional source now of order  $0.4\text{--}0.6\ \mu\text{g kg}^{-1}\ \text{h}^{-1}$ . Hence, we see a seasonal variation of almost an order of magnitude in peak SOA source strength, from maximum in summer to minimum in winter. To put the absolute values of these source strengths in context, note that average modeled concentrations of organic aerosol range  $1\text{--}4\ \mu\text{g kg}^{-1}$ .

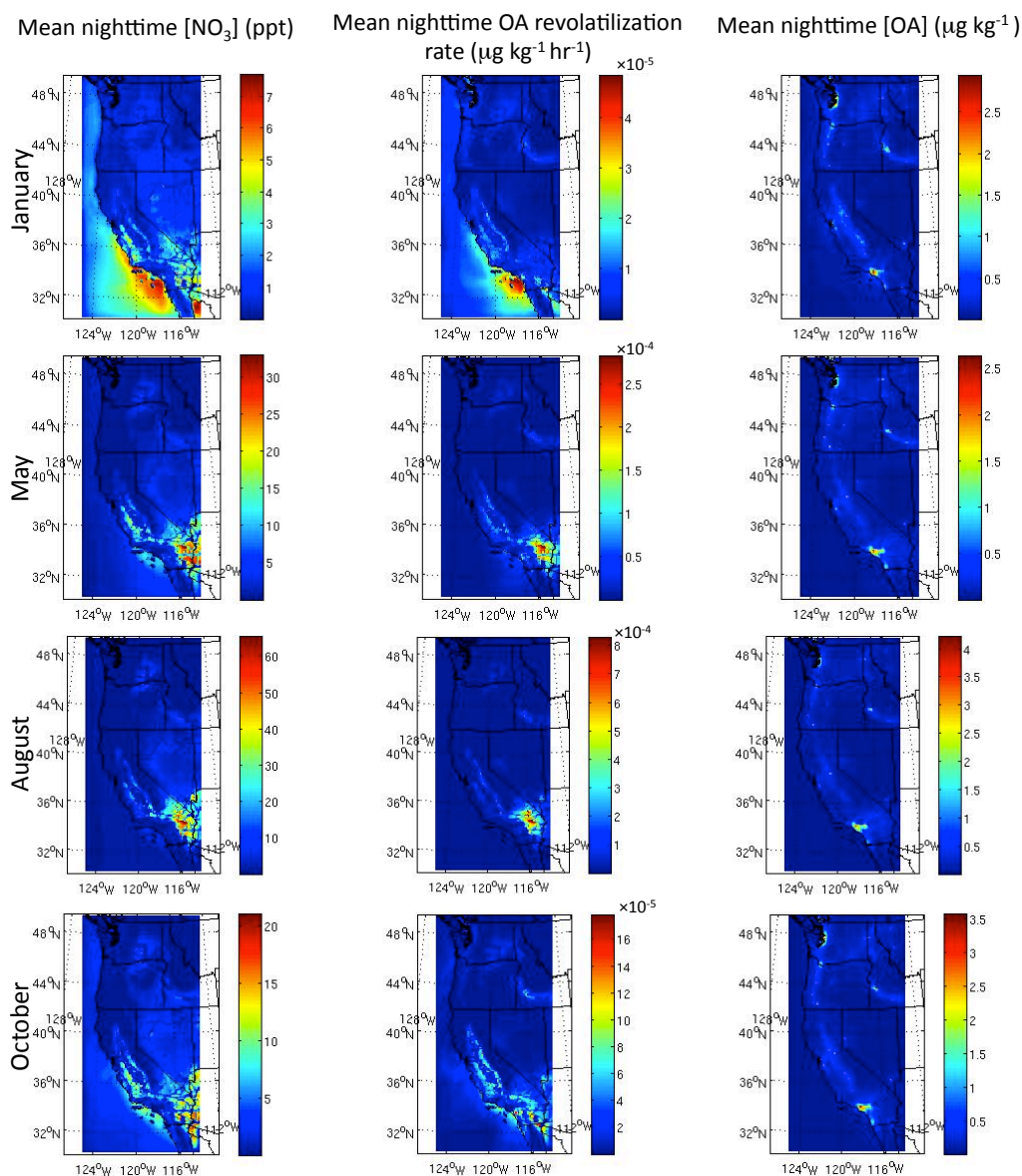


**Fig. 5.** Seasonal pattern of  $\text{NO}_3$ -initiated OA revolatilization (sink) rate (center panels), which is calculated based on the hourly nighttime surface  $[\text{NO}_3]$  map (left panels) and nighttime  $[\text{OA}]$  (right panels). The monthly average of these hourly calculations is shown here.

In all of these simulations, California SOA sources dominate and effectively wash out the smaller source terms downwind of cities in the Pacific Northwest. In Sect. 3.5 below, we will examine a few days of simulation exclusively in this region, to interpret the spatial and temporal variability of this smaller but nevertheless regionally significant SOA source.

### 3.2 Seasonal variation in predicted $\text{NO}_3$ OA sink

Because the organic aerosol peak concentrations in the WRF-Chem model output are more localized to urban areas than reactive organic gases, the  $\text{NO}_3$ -initiated OA sink rates are more localized than the corresponding source terms. Still,

the peaks appear downwind of urban areas where  $\text{NO}_3$  radical concentrations are maximized. Because the peak source and sink terms are co-located with the peak  $[\text{NO}_3]$ , the ratio of these peak concentrations provides a useful metric of the relative importance of  $\text{NO}_3$  as a source and sink of organic aerosol. As shown in Table 2, the predicted SOA source from  $\text{NO}_3$  is three orders of magnitude larger than the  $\text{NO}_3$ -initiated sink throughout the year. Peak revolatilization rates range from  $5 \times 10^{-5} \mu\text{g kg}^{-1} \text{h}^{-1}$  offshore west of Los Angeles in January to  $8 \times 10^{-4} \mu\text{g kg}^{-1} \text{h}^{-1}$  northeast of Los Angeles in August, with highly spatially “focused” patterns, with the exception of October, when the overlap between  $\text{NO}_3$  and OA plumes is minimal, such that regional elevated

revolatilization rates of  $7 \times 10^{-5} \mu\text{g kg}^{-1} \text{h}^{-1}$  are visible in comparison with the downwind of LA peak.

What is the consequence of these rates of revolatilization for OA atmospheric lifetime? For the August Los Angeles peak OA concentration of  $4 \mu\text{g kg}^{-1}$  and peak loss rate of  $8 \times 10^{-4} \mu\text{g kg}^{-1} \text{h}^{-1}$ , the effective organic aerosol lifetime is:

$$\tau_{OA} = \frac{[\text{OA}]}{\text{Loss rate of OA}} \quad (10)$$

giving a lifetime of 5000 h, or 200 days. For comparison, the estimate of OA lifetime with respect to OH revolatilization was  $\approx 6$  days (Molina et al., 2004).

### 3.3 Sensitivity tests, “convergent” assumptions, and speculation on regional importance of source vs. sink

The variability of aerosol formation predicted by the aerosol source program was tested by setting all aerosol yields to 1 %, 5 %, and 95 %. The change in aerosol formation is linearly proportional to the mass yields used.

The variability of the volatilization predicted by the aerosol sink program was tested through several modifications: assuming the greatest possible number of double bonds, using the highest uptake coefficients found in our literature search, setting the fragmentation branching ratio to 0.5 while shrinking other branching ratios proportionally, and multiplying all vapor pressures by  $10^3$ . The fragmentation level of 50 % was considered a good ceiling value, since Knopf et al. (2006) suggest more than 50 % of molecules go through the alcohol + carbonyl channel, and this test addresses the possibility that functionalization may interact with reaction mechanisms to produce increased fragmentation (Kroll et al., 2011). The vapor pressure alteration is based on calculations indicating that adding a carboxylic acid group to a general molecule decreases the vapor pressure by a factor of about  $10^3$  (other functional groups have less impact), adding 5 carbons decreases it by about  $10^2$ , and raising the temperature 10 K increases it by about a factor of 3. Thus, this test imitates the effect of possible errors in aerosol functionalization and carbon number, and temperature variations not accounted for in the fixed vapor pressures. Finally, a “convergent” scenario was run to determine the highest possible sink rate if the errors in all parameters vary in the direction to produce higher sink, using 20 % unsaturation (i.e., 20 % of the surface has alkene uptake coefficient, remaining alkane, using highest uptake coefficients for each), 50 % fragmentation, and vapor pressures increased by a factor of  $10^3$ .

The results of these tests are shown in Table 3. No individual sensitivity test raised the level of revolatilization more than an order of magnitude, and it is noted that manipulations of reactivity (unsaturation and uptake) produced greater changes than manipulations of volatility (fragmentation and

vapor pressures), for a multiplier of 6–10 vs. about 4. Thus, the composition information most important to constraining these results is the quantity and reactivity of double bonds in aerosol, rather than oxidation level or molecular weight.

The “convergent” combined sensitivity test resulted in a substantially higher sink rate, approximately half the source rate obtained with 1 % mass yields. These results indicate that although NO<sub>3</sub> is likely to be a net source of aerosol on the regional scale, it is possible that local conditions may sometimes cause source and sink rates to come into competition, especially since the spatial patterns are not identical. For example, the source term is observed to have substantial contribution from the forested Sierra Nevada mountains around the California central valley, where NO<sub>3</sub> plumes generated downwind of Los Angeles and the San Francisco bay area intercept large terpene emissions. In contrast, in this domain the largest sink contribution is more immediately downwind of urban centers, where anthropogenically produced SOA and NO<sub>3</sub> are both exported in the same plume.

Since this model treats all OA as alike, we cannot identify in our output maps particular types of plumes where heterogeneous loss is more competitive. However, we can speculate on in which air masses this chemistry is likely to be most important based on the factors that the sensitivity tests identified as important. The highest levels of OA unsaturation are likely to occur in regions where SOA is derived from multiple double-bond VOC precursors, such as sesquiterpenes and methyl chavicol on the biogenic side, or aromatics on the anthropogenic side; OA formed from these unsaturated molecules would likely have high reactivity with NO<sub>3</sub>. Fragmentation reactions are favored by molecules with greater functionalization, and therefore a higher oxidation state. Such highly oxidized organic aerosol is observed in more aged aerosol plumes (Kroll et al., 2011); laboratory studies indicate that only 1–4 generations of oxidation are required before fragmentation becomes competitive. Hence, the NO<sub>3</sub>-initiated heterogeneous OA loss is predicted to be most important in aged, oxidant influenced, heavier terpene-rich biogenic or aromatic-rich anthropogenic plumes. All products will be more volatile in regions with higher temperature, so warmer nights would further favor this sink process.

Some limitations of our product generation scheme should be noted. First, functional group composition is strictly additive. There is no provision, for example, for a carbonylation reaction to take place at the carbon of a terminal alcohol and produce a carboxylic acid. Second, it is assumed that the product branching ratios and double bond reactivity are independent of carbon number. Because small oxidized molecules have a higher percentage of quaternary carbons than equally functionalized long-chain molecules, they may have reduced uptake, but our model does not capture this.

**Table 3.** Results of model sensitivity tests.

Modification	Maximum January aerosol loss rate (L.A. plume, $\mu\text{g kg}^{-1} \text{h}^{-1}$ )	Maximum January aerosol formation rate (L.A. plume, $\mu\text{g kg}^{-1} \text{h}^{-1}$ )
Unmodified source	–	0.4
All mass yields 1 %	–	0.011
All mass yields 5 %	–	0.06
All mass yields 95 %	–	1.1
Unmodified sink	$9.6 \times 10^{-5}$	–
Maximum uptake coefficient	$8.3 \times 10^{-4}$	–
50 % fragmentation	$3.4 \times 10^{-4}$	–
All vapor pressures $\times 10^3$	$3.2 \times 10^{-4}$	–
Maximum uptake coefficients (see text)	$5.9 \times 10^{-4}$	–
“Convergent” assumptions	Maximum August aerosol loss rate (L.A. plume, $\mu\text{g kg}^{-1} \text{h}^{-1}$ )	Maximum August aerosol formation rate (L.A. plume, $\mu\text{g kg}^{-1} \text{h}^{-1}$ )
1 % mass yields	–	0.09
20 % unsaturated, maximum uptake coefficients, 50 % fragmentation, vapor pressures $\times 10^3$	0.045	–

### 3.4 Effect of heterogeneous $\text{NO}_3$ loss on nighttime $\text{NO}_y$ budget

The above analysis, showing modeled total OA sink rates typically several orders of magnitude lower than the corresponding source terms, suggests that atmospheric  $\text{NO}_3$  is much more important for aerosol production than its heterogeneous revolatilization. Still, this heterogeneous uptake on the surface of existing organic aerosol may be important for the nighttime budget of oxidized nitrogen species ( $\text{NO}_y$ ) by providing a loss term for  $\text{NO}_3$ . To assess the importance of this process, we plot the loss rate of  $\text{NO}_3$  in ppt  $\text{hr}^{-1}$  in Figure 6. Again, the peak importance of this process occurs downwind of Los Angeles, with a maximum loss rate of 1.4 ppt  $\text{hr}^{-1}$  in August. This corresponds to an August minimum in nitrate lifetime, calculated analogously to the OA lifetime in Eqn. 10, of 50 ppt / 1.4 ppt  $\text{hr}^{-1} = 36$  h. Because  $\text{NO}_3$  is photolyzed rapidly every sunrise, this loss process does not significantly limit the lifetime of  $\text{NO}_3$  radical throughout most of the troposphere. In any region where alkenes are present,  $\text{NO}_3$  homogeneous reaction will be more important than heterogeneous reaction:  $\text{NO}_3$  reactivity is much higher with gas-phase alkenes. For example, the  $\text{NO}_3$  lifetime with respect to reaction with  $\alpha$ -pinene present at a typical concentration of 100 ppt would be 70 s ( $k_{\text{NO}_3+\alpha\text{pin}} = 6 \times 10^{-12} \text{ cm}^3 \text{ molec}^{-1} \text{ s}^{-1}$ , Calvert et al. (2000)).

### 3.5 Night-to-night variability in spatial patterns

Because meteorology and emissions vary day-to-day, the monthly averaged results necessarily present dampened max-

ima relative to individual nightly data, which have varying peak intensity and location. Several individual nightly averages are shown in Figs. 7–10 to illustrate this variability. We also plot several individual nights’ maps for source and sink rates zoomed in on only the Pacific Northwest, to highlight spatial and temporal variability, as well as the overall magnitudes of these processes without the washing-out effect of including the California cities on the same z-axis.

In the SOA source maps (Figs. 7 and 8), most nightly maxima are significantly higher (up to a factor of three) than the monthly average, with large spatial variation in peak location primarily responsible for the monthly averages being lower. For example, Fig. 7 shows a day (12 August) when Las Vegas’ plume dominates the entire west coast domain, three days when the San Francisco/Sacramento plume competes with that of Los Angeles (14–16 August), two days when Seattle competes (16–17 August), as well as the large night-to-night variation in the shape of the Los Angeles source plume.

In the OA sink maps (Figs. 9 and 10), less spatial variation is obvious, suggesting that the location of organic aerosol plume is more constant than reactive organic gases. There is more variability in magnitude than spatial patterns, with an apparently wider distribution around the monthly average than in the source model.

In both source and sink maps, more spatial variation is apparent in the (overall lower) rates for the smaller Pacific Northwest domain (Figs. 8 and 10). In these zoomed maps, the occasionally significant  $\text{NO}_3$  SOA source rates for the Portland metropolitan area, Spokane, WA, and Boise, ID are apparent. There is a region of higher organic aerosol in southeastern Washington which occasionally overlaps a large  $\text{NO}_x$

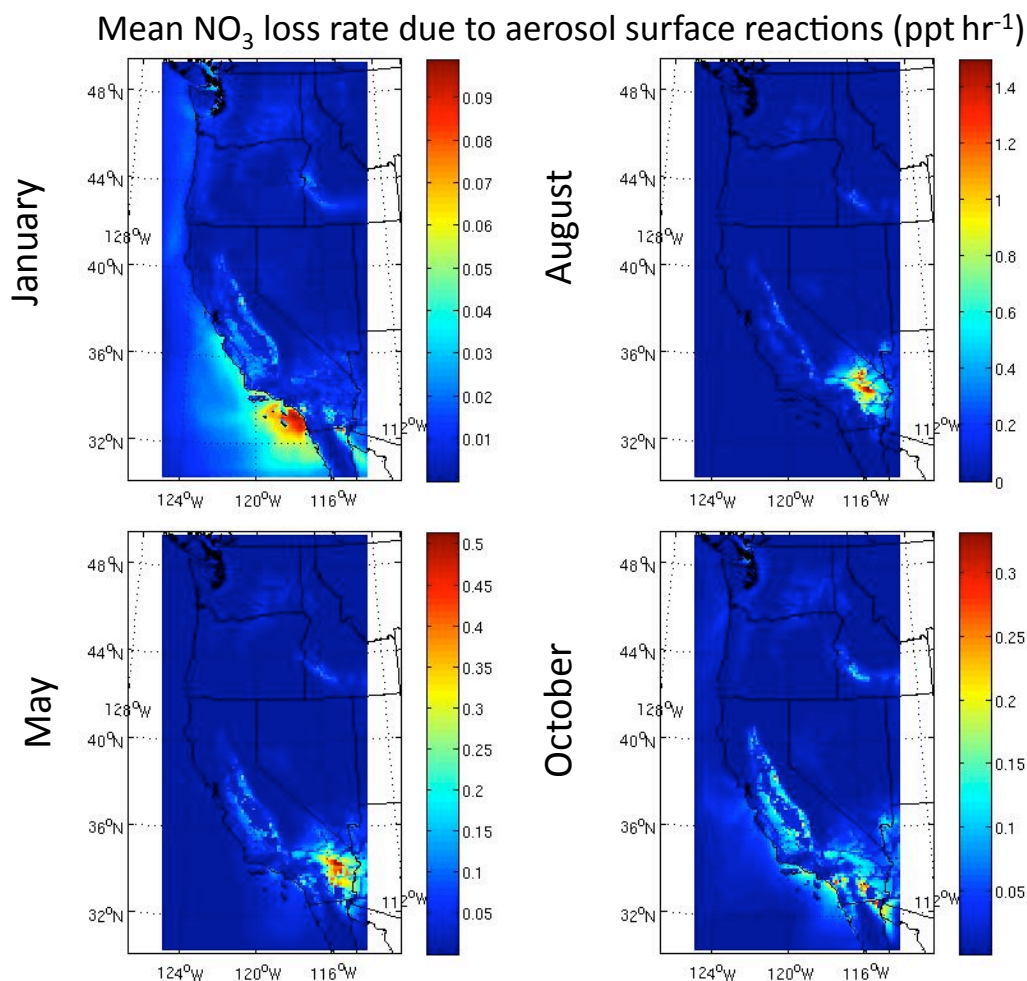


**Fig. 6.** Seasonal pattern of  $\text{NO}_3$  loss rate as a result of heterogeneous reactions on OA surfaces.

plume from the Boardman coal-fired power plant along the Columbia River in Boardman, OR, giving sporadically larger OA loss rates in that region. Boise's urban plume dominates on other days.

### 3.6 Atmospheric relevance

To put these results into context, we seek to compare the  $\text{NO}_3$ -initiated OA production rates determined here to other studies of SOA sources. Results available from global and regional studies are often reported in terms of surface OA concentrations from various formation mechanisms (Robinson et al., 2007; Pye et al., 2010) or in terms of total global sources in  $\text{TgC yr}^{-1}$  (Hallquist et al., 2009). We note again, however, that our modeling is based strictly on offline calculations of source and sink rates of  $\text{NO}_3$ , not allowing products of these reactions to accumulate or interact with the chemistry in the regional model. As such we can base comparisons only on the instantaneous rates of these processes.

Two recent studies of SOA production mechanisms have reported peak surface concentrations of organic aerosol of

up to  $4 \mu\text{g m}^{-3}$  over urban areas in the eastern US from “traditional” SOA precursors (Robinson et al., 2007), and up to  $3.35 \mu\text{g m}^{-3}$  over the US from  $\text{NO}_3$  + monoterpenes and isoprene in August (Pye et al., 2010). These numbers can be qualitatively compared to the OA source rate determined here by assuming an aerosol lifetime and steady-state concentration. Our results suggest a peak SOA source of  $3 \mu\text{g kg}^{-1} \text{h}^{-1}$  and more representative regionally distributed source of order  $0.2\text{--}0.4 \mu\text{g kg}^{-1} \text{h}^{-1}$  for the month of August. These regional numbers can be converted to increases in surface OA concentration in  $\mu\text{g m}^{-3}$  using the density of dry air ( $1.2 \text{ kg m}^{-3}$ ) and an estimated OA lifetime, using equation 10. The lifetime of organic aerosol has been estimated to be 4 days (Liousse et al., 1996), assuming wet deposition to be the dominant sink. This gives regional SOA source rates of  $0.24\text{--}0.48 \mu\text{g m}^{-3} \text{h}^{-1}$ , which would correspond to increases in OA concentration of  $23\text{--}46 \mu\text{g m}^{-3}$  at peak nighttime production in areas where this  $\text{NO}_3$ -initiated SOA chemistry is important (aqua and “hotter” colored regions in Fig. 4). This large additional source estimate, an order of magnitude larger

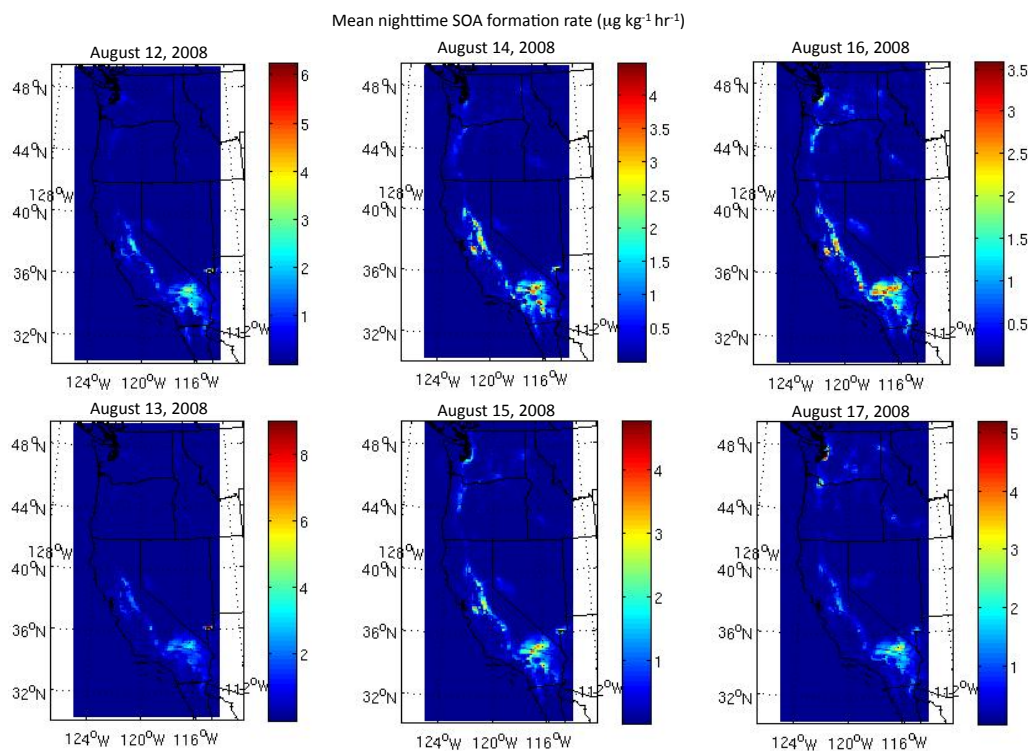


**Fig. 7.** Several individual nights' averages of the  $\text{NO}_3$ -initiated SOA source, showing spatial and magnitude variability for the western United States domain.

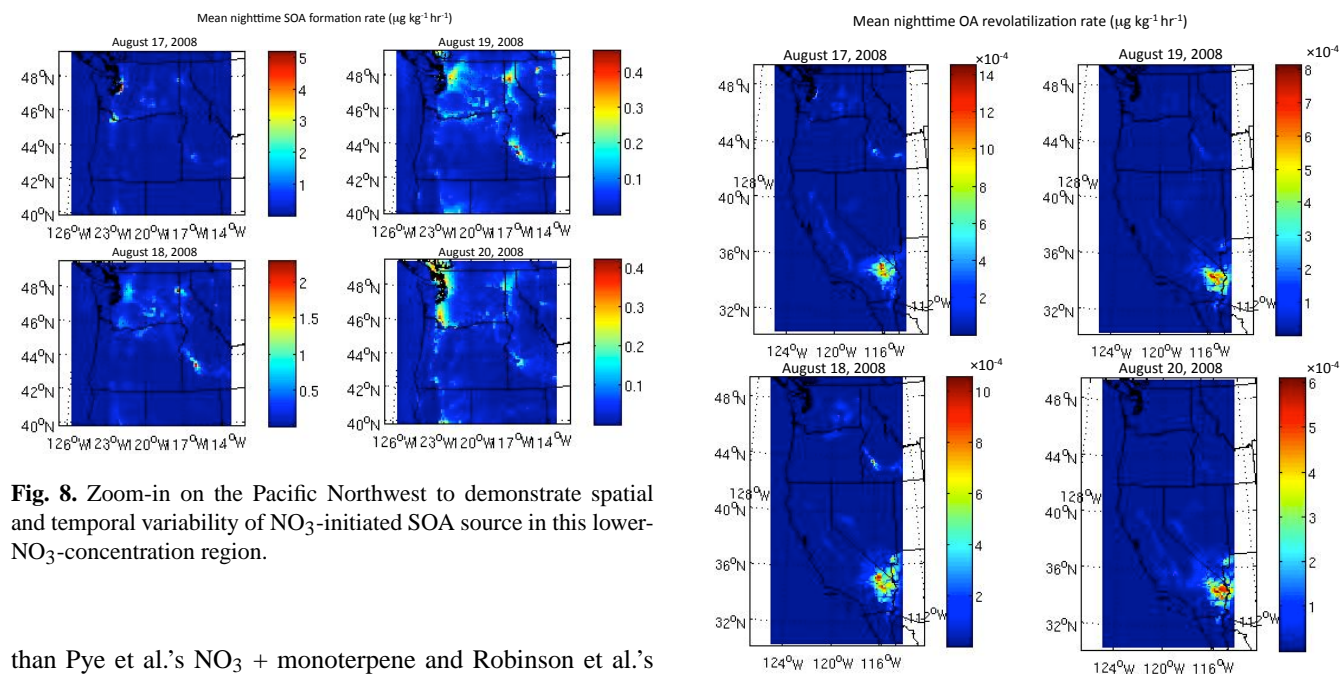


**Fig. 8.** Zoom-in on the Pacific Northwest to demonstrate spatial and temporal variability of  $\text{NO}_3$ -initiated SOA source in this lower- $\text{NO}_3$ -concentration region.

**Fig. 9.** Several individual night's averages of the  $\text{NO}_3$ -initiated OA loss, showing spatial and magnitude variability for the western United States domain.

than Pye et al.'s  $\text{NO}_3$  + monoterpene and Robinson et al.'s traditional SOA estimates, suggests that this crude lifetime analysis overestimates this source, but nevertheless that this mechanism is likely to be significant regionally.

An alternative method of comparison is to calculate for our model domain the total additional OA source predicted in  $\text{TgC yr}^{-1}$  and compare to global estimates of SOA source.

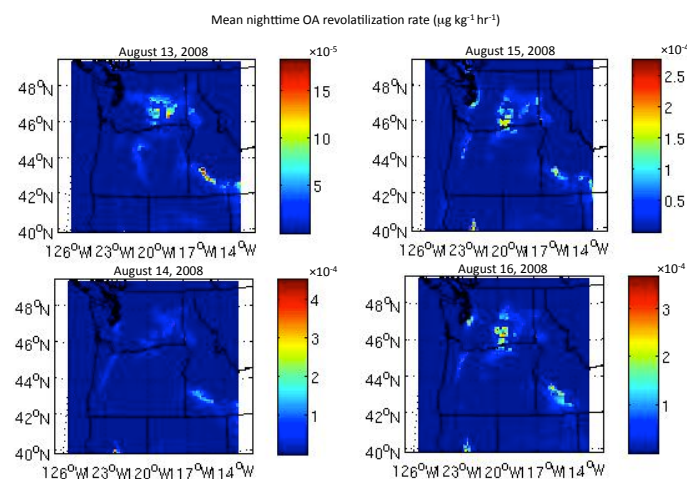


**Fig. 10.** Zoom-in on the Pacific Northwest to demonstrate spatial and temporal variability of NO<sub>3</sub> OA loss in this lower-NO<sub>3</sub>-concentration region.

Global estimates of anthropogenic SOA and biogenic SOA are 2–12 Tg yr<sup>-1</sup> (Henze et al., 2008) and 13–70 Tg yr<sup>-1</sup> (Kanakidou et al., 2005) respectively. These numbers refer to total organic aerosol mass, assuming a ratio of 1.4 organic matter to organic carbon. In our model for the month of August, summed averaged surface OA source from NO<sub>3</sub> + reactive organic gases in the western US domain is 1.4 Tg yr<sup>-1</sup> (average nighttime production rate of 0.0894 µg m<sup>-3</sup> h<sup>-1</sup> over a domain area of 2.3 × 10<sup>15</sup> m<sup>2</sup>, with mean lowest layer height of 790 m).

Both of these model-derived source estimates are necessarily overestimates, because this offline calculation does not consume NO<sub>3</sub> radical, ROG, or OA in the model at each time step. However, our model results clearly demonstrate that the source greatly exceeds any heterogeneous sink initiated by NO<sub>3</sub>. Furthermore, the large magnitude of the predicted SOA source relative to global estimates suggests that this process should be included online in models. Only with such direct inclusion will it be possible to definitively assess the importance of this process in terms of OA production and as a NO<sub>3</sub> radical sink.

#### 4 Conclusions

NO<sub>3</sub> radical-initiated chemistry is predicted to be significantly more important as a *source* of organic aerosol than as a heterogeneous *sink* of organic aerosol in the western United States. However, significant spatial and day-to-day variability in modeled source and sink suggest that both processes are important in certain locations at some times, in particular, downwind of urban areas on summer nights when terpene emissions have been large. Comparison of the average modeled NO<sub>3</sub> + alkene source for the western United States to other regional and global predictions of total organic aerosol

loading suggests that this process may be an important contributor to both OA and nitrate radical budgets. Better constraints on the importance of the heterogeneous OA sink rate require improved knowledge of the number and reactivity of double bonds in ambient aerosol. Online calculations including this NO<sub>3</sub> chemistry are required to determine the quantitative importance of both source and sink processes.

**Supplementary material related to this article is available online at:** <http://www.atmos-chem-phys.net/12/8797/2012/acp-12-8797-2012-supplement.pdf>.

**Acknowledgements.** The WRF-Chem model runs were performed using EMSL (project # 30394), a national scientific user facility sponsored by the Department of Energy's Office of Biological and Environmental Research and located at Pacific Northwest National Laboratory. The authors gratefully acknowledge helpful discussions with Jerome Fast (PNNL) while setting up the model. We thank the reviewers for thoughtful critiques that have helped us improve this modeling study, and Dan Chen (UCLA) for providing maps of Los Angeles area anthropogenic and biogenic OLT and OLI emissions to help us address potential BVOC interferences.

Edited by: J. B. Burkholder

#### References

- Alves, C., Pio, C., and Duarte, A.: Composition of extractable organic matter of air particles from rural and urban Portuguese area, *Atmos. Environ.*, 35, 5485–5496, 2001.
- Atkinson, R. and Arey, J.: Gas-phase tropospheric chemistry of biogenic volatile organic compounds: a review, *Atmos. Environ.*, 37, Supplement 2, 197–219, doi:10.1016/S1352-2310(03)00391-1, 2003.
- Baduel, C., Voisin, D., and Jaffrezo, J.-L.: Seasonal variation of concentrations and optical properties of water soluble HULIS collected in urban environments, *Atmos. Chem. Phys.*, 10, 4085–4095, doi:10.5194/acp-10-4085-2010, 2010.
- Calvert, J., Atkinson, J., Kerr, J., Madronich, S., Moortgat, G. K., Wallington, T., and Yarwood, G.: Mechanisms of the atmospheric oxidation of the alkenes, Oxford University Press, New York, NY, USA, 127–171, 2000.
- Fry, J. L., Kiendler-Scharr, A., Rollins, A. W., Wooldridge, P. J., Brown, S. S., Fuchs, H., Dubé, W., Mensah, A., dal Maso, M., Tillmann, R., Dorn, H.-P., Brauers, T., and Cohen, R. C.: Organic nitrate and secondary organic aerosol yield from NO<sub>3</sub> oxidation of β-pinene evaluated using a gas-phase kinetics/aerosol partitioning model, *Atmos. Chem. Phys.*, 9, 1431–1449, doi:10.5194/acp-9-1431-2009, 2009.
- Grell, G. A., Peckham, S. E., Schmitz, R., McKeen, S. A., Frost, G., Skamarock, W. C., and Eder, B.: Fully coupled online chemistry within the WRF model, *Atmos. Environ.*, 39, 6957–6975, doi:10.1016/j.atmosenv.2005.04.027, 2005.

- Griffin, R. J., Flagan, R. C., and Seinfeld, J. H.: Organic aerosol formation from the oxidation of biogenic hydrocarbons, *J. Geophys. Res.*, 104, 3555–3568, doi:10.1029/1998JD100049, 1999.
- Gross, S. and Bertram, A. K.: Reactive Uptake of NO<sub>3</sub>, N<sub>2</sub>O<sub>5</sub>, NO<sub>2</sub>, HNO<sub>3</sub>, and O<sub>3</sub> on Three Types of Polycyclic Aromatic Hydrocarbon Surfaces, *J. Phys. Chem. A*, 112, 3104–3113, doi:10.1021/jp7107544, PMID: 18311955, 2008.
- Gross, S., Iannone, R., Xiao, S., and Bertram, A. K.: Reactive uptake studies of NO<sub>3</sub> and N<sub>2</sub>O<sub>5</sub> on alkenoic acid, alkanolate, and polyalcohol substrates to probe nighttime aerosol chemistry, *Phys. Chem. Chem. Phys.*, 11, 7792–7803, doi:10.1039/B904741G, 2009.
- Guenther, A., Zimmerman, P., Harley, P., Monson, R., and Fall, R.: Isoprene and Monoterpene Emission Rate Variability: Model Evaluations and Sensitivity Analyses, *J. Geophys. Res.*, 98, 12609–12617, 1993.
- Guenther, A., Zimmerman, P., and Wildermuth, M.: Natural volatile organic compound emission rate estimates for U.S. woodland landscapes, *Atmos. Environ.*, 28, 1197–1210, doi:10.1016/1352-2310(94)90297-6, 1994.
- Guenther, A., Karl, T., Harley, P., Wiedinmyer, C., Palmer, P. I., and Geron, C.: Estimates of global terrestrial isoprene emissions using MEGAN (Model of Emissions of Gases and Aerosols from Nature), *Atmos. Chem. Phys.*, 6, 3181–3210, doi:10.5194/acp-6-3181-2006, 2006.
- Hallquist, M., Wangberg, I., Ljungstrom, E., Barnes, I., and Becker, K. H.: Aerosol and product yields from NO<sub>3</sub> radical-initiated oxidation of selected monoterpenes, *Environ. Sci. Technol.*, 33, 553–559, 1999.
- Hallquist, M., Wenger, J. C., Baltensperger, U., Rudich, Y., Simpson, D., Claeys, M., Dommen, J., Donahue, N. M., George, C., Goldstein, A. H., Hamilton, J. F., Herrmann, H., Hoffmann, T., Iinuma, Y., Jang, M., Jenkin, M. E., Jimenez, J. L., Kiendler-Scharr, A., Maenhaut, W., McFiggans, G., Mentel, Th. F., Monod, A., Prévôt, A. S. H., Seinfeld, J. H., Surratt, J. D., Szmigielski, R., and Wildt, J.: The formation, properties and impact of secondary organic aerosol: current and emerging issues, *Atmos. Chem. Phys.*, 9, 5155–5236, doi:10.5194/acp-9-5155-2009, 2009.
- Hamilton, J. F., Webb, P. J., Lewis, A. C., Hopkins, J. R., Smith, S., and Davy, P.: Partially oxidised organic components in urban aerosol using GCXGC-TOF/MS, *Atmos. Chem. Phys.*, 4, 1279–1290, doi:10.5194/acp-4-1279-2004, 2004.
- Hamilton, J. F., Lewis, A. C., Reynolds, J. C., Carpenter, L. J., and Lubben, A.: Investigating the composition of organic aerosol resulting from cyclohexene ozonolysis: low molecular weight and heterogeneous reaction products, *Atmos. Chem. Phys.*, 6, 4973–4984, doi:10.5194/acp-6-4973-2006, 2006.
- Henze, D. K., Seinfeld, J. H., Ng, N. L., Kroll, J. H., Fu, T.-M., Jacob, D. J., and Heald, C. L.: Global modeling of secondary organic aerosol formation from aromatic hydrocarbons: high- vs. low-yield pathways, *Atmos. Chem. Phys.*, 8, 2405–2420, doi:10.5194/acp-8-2405-2008, 2008.
- IPCC: Climate Change 2007 – The Physical Science Basis: Working Group I Contribution to the Fourth Assessment Report of the IPCC, Cambridge University Press, Cambridge, UK and New York, NY, USA, 2007.
- Kanakidou, M., Seinfeld, J. H., Pandis, S. N., Barnes, I., Dentener, F. J., Facchini, M. C., Van Dingenen, R., Ervens, B., Nenes, A., Nielsen, C. J., Swietlicki, E., Putaud, J. P., Balkanski, Y., Fuzzi, S., Horth, J., Moortgat, G. K., Winterhalter, R., Myhre, C. E. L., Tsigaridis, K., Vignati, E., Stephanou, E. G., and Wilson, J.: Organic aerosol and global climate modelling: a review, *Atmos. Chem. Phys.*, 5, 1053–1123, doi:10.5194/acp-5-1053-2005, 2005.
- Karydis, V. A., Tsimpidi, A. P., and Pandis, S. N.: Evaluation of a three-dimensional chemical transport model (PMCAMx) in the eastern United States for all four seasons, *J. Geophys. Res. Atmos.*, 112, D14211, doi:10.1029/2006JD007890, 2007.
- Knopf, D., Mak, J., Gross, S., and Bertram, A.: Does atmospheric processing of saturated hydrocarbon surfaces by NO<sub>3</sub> lead to volatilization?, *Geophys. Res. Lett.*, 33, L17816, doi:10.1029/2006GL026884, 2006.
- Kroll, J., Donahue, N., Jimenez, J., Kessler, S., Canagaratna, M., Wilson, K., Altieri, K., Mazzoleni, L., Wozniak, A., Bluhm, H., Mysak, E., Smith, J., Kolb, C., and Worsnop, D.: Carbon oxidation state as a metric for describing the chemistry of atmospheric organic aerosol, *Nature Chem.*, 3, 133–139, doi:10.1038/nchem.948, 2011.
- Lioussé, C., Penner, J. E., Chuang, C., Walton, J. J., Eddleman, H., and Cachier, H.: A global three-dimensional model study of carbonaceous aerosols, *J. Geophys. Res.*, 107, 19411–19432, doi:10.1029/95JD03426, 1996.
- Moise, T., Talukdar, R. K., Frost, G. J., Fox, R. W., and Rudich, Y.: Reactive uptake of NO<sub>3</sub> by liquid and frozen organics, *J. Geophys. Res.*, 101, L05811, doi:10.1029/2001JD000334, 2002.
- Molina, M. J., Ivanov, A. V., Trakhtenberg, S., and Molina, L. T.: Atmospheric evolution of organic aerosol, *Geophys. Res. Lett.*, 312, L22104, doi:10.1029/2004GL020910, 2004.
- Ng, N. L., Kwan, A. J., Surratt, J. D., Chan, A. W. H., Chhabra, P. S., Sorooshian, A., Pye, H. O. T., Crouse, J. D., Wennberg, P. O., Flagan, R. C., and Seinfeld, J. H.: Secondary organic aerosol (SOA) formation from reaction of isoprene with nitrate radicals (NO<sub>3</sub>), *Atmos. Chem. Phys.*, 8, 4117–4140, doi:10.5194/acp-8-4117-2008, 2008.
- Odum, J. R., Hoffmann, T., Bowman, F., Collins, D., Flagan, R. C., and Seinfeld, J. H.: Gas/Partitioning and Secondary Organic Aerosol Yields, *Environ. Sci. Technol.*, 30, 2580–2585, 1996.
- Pankow, J. F. and Asher, W. E.: SIMPOL.1: a simple group contribution method for predicting vapor pressures and enthalpies of vaporization of multifunctional organic compounds, *Atmos. Chem. Phys.*, 8, 2773–2796, doi:10.5194/acp-8-2773-2008, 2008.
- Pope, C. and Dockery, D.: Critical Review: Health Effects of Fine Particulate Air Pollution: Lines that Connect, *J. Air Waste Manage. Assoc.*, 6, 709–742, 2006.
- Pye, H. O. T., Chan, A. W. H., Barkley, M. P., and Seinfeld, J. H.: Global modeling of organic aerosol: the importance of reactive nitrogen (NO<sub>x</sub> and NO<sub>3</sub>), *Atmos. Chem. Phys.*, 10, 11261–11276, doi:10.5194/acp-10-11261-2010, 2010.
- Robinson, A. L., Donahue, N. M., Shrivastava, M. K., Weitkamp, E. A., Sage, A. M., Grieshop, A. P., Lane, T. E., Pierce, J. R., and Pandis, S. N.: Rethinking Organic Aerosols: Semivolatile Emissions and Photochemical Aging, 315, 1259–1262, doi:10.1126/science.1133061, 2007.
- Rollins, A. W., Kiendler-Scharr, A., Fry, J. L., Brauers, T., Brown, S. S., Dorn, H.-P., Dubé, W. P., Fuchs, H., Mensah, A., Mentel, T. F., Rohrer, F., Tillmann, R., Wegener, R., Wooldridge, P. J., and

- Cohen, R. C.: Isoprene oxidation by nitrate radical: alkyl nitrate and secondary organic aerosol yields, *Atmos. Chem. Phys.*, 9, 6685–6703, doi:10.5194/acp-9-6685-2009, 2009.
- Schoenemeyer, T., Richter, K., and Smiatek, G.: Vorstudie über ein räumlich und zeitlich aufgelöstes Kataster anthropogener und biogener Emissionen für Bayern mit Entwicklung eines Prototyps und Anwendung für Immissionsprognosen: Abschlussbericht an das Bayerische Landesamt für Umweltschutz, Tech. rep., Fraunhofer-Institut für Atmosphärische Umweltforschung, Garmisch-Partenkirchen, 1997.
- Simpson, D., Guenther, A., Hewitt, C. N., and Steinbrecher, R.: Biogenic emissions in Europe 1. Estimates and uncertainties, *J. Geophys. Res.*, 100, 22875–22890, doi:10.1029/95JD02368, 1995.
- Spittler, M., Barnes, I., Bejan, I., Brockmann, K. J., Benter, T., and Wirtz, K.: Reactions of NO<sub>3</sub> radicals with limonene and alpha-pinene: Product and SOA formation, *Atmos. Environ.*, 40, S116–S127, doi:10.1016/j.atmosenv.2005.09.093, 2006.
- Watson, J.: Critical Review –Visibility: Science and Regulation, *J. Air Waste Manage. Assoc.*, 52, 628–713, 2002.
- Wild, O., Zhu, X., and Prather, M.: Fast-J: Accurate Simulation of In- and Below-Cloud Photolysis in Tropospheric Chemical Models, *J. Atmos. Chem.*, 37, 245–282, 2000.
- Yu, S., Dennis, R., Roselle, S., Nenes, A., Walker, J., Eder, B., Schere, K., Swall, J., and Robarge, W.: An assessment of the ability of three-dimensional air quality models with current thermodynamic equilibrium models to predict aerosol NO<sub>3</sub><sup>-</sup>, *J. Geophys. Res. Atmos.*, 110, D07S13, doi:10.1029/2004JD004718, 2005.
- Zaveri, R. A. and Peters, L. K.: A new lumped structure photochemical mechanism for large-scale applications, *J. Geophys. Res.*, 1043, 30387–30416, doi:10.1029/1999JD900876, 1999.
- Zaveri, R. A., Easter, R. C., Fast, J. D., and Peters, L. K.: Model for Simulating Aerosol Interactions and Chemistry (MOSAIC), *J. Geophys. Res.*, 113, D13204, doi:10.1029/2007JD008782, 2008.
- Zhang, Q., Jimenez, J. L., Canagaratna, M. R., Allan, J. D., Coe, H., Ulbrich, I., Alfarra, M. R., Takami, A., Middlebrook, A. M., Sun, Y. L., Dzepina, K., Dunlea, E., Docherty, K., DeCarlo, P. F., Salcedo, D., Onasch, T., Jayne, J. T., Miyoshi, T., Shimojo, A., Hatakeyama, S., Takegawa, N., Kondo, Y., Schneider, J., Drewnick, F., Borrmann, S., Weimer, S., Demerjian, K., Williams, P., Bower, K., Bahreini, R., Cottrell, L., Griffin, R. J., Rautiainen, J., Sun, J. Y., Zhang, Y. M., and Worsnop, D. R.: Ubiquity and dominance of oxygenated species in organic aerosols in anthropogenically-influenced Northern Hemisphere midlatitudes, *Geophys. Res. Lett.*, 34, L13801, doi:10.1029/2007GL029979, 2007.